Flow of particles suspended in a sheared viscous fluid: Effects of finite inertia and inelastic collisions

Micheline Abbas, Eric Climent, Jean-François Parmentier, Olivier Simonin

Flow of Particles Suspended in a Sheared Viscous Fluid: Effects of Finite Inertia and Inelastic Collisions

Micheline Abbas and Eric Climent
Université de Toulouse, INPT - UPS, Laboratoire de Génie Chimique, F-31432 Toulouse, France, and CNRS, Fédération de Recherche FERMaT, F-31432 Toulouse, France

Jean-François Parmentier and Olivier Simonin
Université de Toulouse, INPT - UPS, Institut de Mécanique des Fluides, F-31400 Toulouse, France, and CNRS, Fédération de Recherche FERMaT, F-31400 Toulouse, France

We investigate in this article the macroscopic behavior of sheared suspensions of spherical particles. The effects of the fluid inertia, the Brownian diffusion, and the gravity are neglected. We highlight the influence of the solid-phase inertia on the macroscopic behavior of the suspension, considering moderate to high Stokes numbers. Typically, this study is concerned with solid particles O *(100 μm) suspended in a gas with a concentration varying from 5% to 30%. A hard-sphere collision model (with elastic or inelasic rebounds) coupled with the particle Lagrangian tracking is used to simulate the suspension dynamics in an unbounded periodic domain. We first consider the behavior of the suspension with perfect elastic collisions. The suspension properties reveal a strong dependence on the particle inertia and concentration. Increasing the Stokes number from 1 to 10 induces an enhancement of the particle agitation by three orders of magnitude and an evolution of the probability density function of the fluctuating velocity from a highly peaked (close to the Dirac function) to a Maxwellian shape. This sharp transition in the velocity distribution function is related to the time scale which controls the overall dynamics of the suspension flow. The particle relaxation (resp. collision) time scale dominates the particulate phase behavior in the weakly (resp. highly) agitated suspensions. The numerical results are compared with the prediction of two statistical models based on the kinetic theory for granular flows adapted to moderately inertial regimes. The suspensions have a Newtonian behavior when they are highly agitated similarly to rapid granular flows. However, the stress tensors are highly anisotropic in weakly agitated suspensions as a difference of normal stresses arises. Finally, we discuss the effect of energy dissipation due to inelastic collisions on the statistical quantities. We also tested the influence of a simple modeling of local hydrodynamic interactions during the collision by using a restitution coefficient which depends on the local impact velocities.*
AIChE J, 56: 2523–2538, 2010

Introduction

Gas–solid flows are encountered in many industrial processes: fuel combustion, pneumatic conveying of particles, catalytic cracking fluidization, particle separators like cyclones,…. They may be also encountered in a natural environment like sand storms, moving sand dunes, avalanches. Optimum designs of the industrial processes or reliable predictions of natural phenomena may be achieved when the physics governing these particulate flows will be thoroughly understood and accuretaly modeled.[1,2] Usual designs of engineering configurations are often based on empirical rules and modeling. The purpose of our study is to contribute to developing and validating macroscopic models recommended for gas–solid suspension flows. In this context, we propose to analyze discrete particle simulations leading to detailed information about the statistical behavior of the suspension which otherwise might be difficult to obtain in physical experiments.[3,4] The statistics based on the individual tracking of all the particles can then be compared with theoretical predictions for validation and improvement of closure models useful for the computational fluid dynamics of practical applications.

Our study is focused on homogeneous gas–solid flows, particularly sheared suspensions. Because of the combined effects of inertia and collisons, the instantaneous slip velocity between the particles and the carrying fluid flow is significant. We consider that the particle/particle interactions are dominated by collisions and that the particle/fluid interaction is simply modeled by the Stokes drag valid for low Reynolds numbers. Gas–solid or liquid–solid fluidized beds are typical configurations where the suspension dynamics is controlled by both the drag force and collisions in addition to the gravity forcing.[5–7]

Whereas most of the real flows encountered in industry (milling, fluidization, and filtration processes) are facing complicated time and space velocity gradients, we choose to emphasize the response of the suspension to a simple linear shear flow as a prototype configuration. Also, we neglect gravity to disentangle the effects of a mean slip velocity and the agitation induced by the presence of the shear flow.

The relative importance of the different relevant phenomena in flows of suspension can be expressed in terms of dimensionless numbers. The particle inertia is characterized by the Stokes number $St = \tau_p/\tau_f$. This dimensionless number compares the fluid characteristic time scale τ_f (equal to γ^{-1} in a shear flow where γ is the local shear rate) and the viscous particulate relaxation time $\tau_p = 2\rho_p a^2/9\mu_f$ (where ρ_p and a stand, respectively, for the particle density and radius; μ_f is the dynamic fluid viscosity). The viscous stress is compared with the fluid inertia in the Reynolds number $Re = \rho_f \gamma a^2/\mu_f$. Advection of the particles and thermal agitation are compared in the Péclet number $Pe = \gamma a^2/(k_B T/6\pi\mu a)$ where the diffusion coefficient has been approximated by Stokes-Einstein's law for an isolated particle. Practically, the dimensionless numbers depend on the particle size and density in a uniformly sheared suspension ($\gamma = 10\ s^{-1}$ is a typical shear rate of classical applications) for fixed properties of the gas. In Figure 1, we chose the gas to be air and varied the physical properties (size and density) of the particles within engineering applications (ranging from powder of wood coal to uranium particles). Horizontal dashed lines correspond to certain types of material and different sizes of particle. Solid lines correspond, respectively, to the dimensionless *St, Re*, and *Pe* numbers equal to unity. Constant Péclet and Reynolds numbers are vertical lines as they depend only on the particle radius and not on the particle density. The range of particle radius subject to Brownian motion is located on the left side of the line $Pe = 1$ and macroscopic particles are located on the right. On the left of the line $St = 1$, the particle trajectories are weakly influenced by inertia effects, whereas the suspension may be called inertial on the right side of this line. For the line $Re = 1$, suspensions standing on the left are described by the Stokes equations (creeping flow), whereas the Navier-Stokes equations hold on the right of this line. The *Ar* number which measures the influence of buoyancy is not shown in this figure because for this range of particle density, the particles are always much influenced by gravity. But we chose to neglect the settling of the suspension to emphasize the effect of shear. We consider suspensions with moderate inertia in the limit of vanishing Reynolds numbers and Brownian diffusion. Consequently, the range of particle radius and densities lie between the lines $St = 1$ and $Re = 1$ in Figure 1.

The shear flow promotes local particle encounters. Hence, interparticle but also fluid-particle interactions generate velocity fluctuations in the particulate phase. These microscopic fluctuations induce momentum and possibly mass transfer (if the suspension is not homogensous) on a larger scale. In the regime of infinite inertia of the dispersed phase ($St \to \infty$), the suspensions behave like a dry granular material. Particles fly along straight lines between successive collisions following random paths. The dynamics of nearly elastic particles driven by collisions is similar to those of the molecules in a hard-sphere gas which was traditionaly described by a statistical approach based on the kinetic theory. This theory relies on a statistical approach for an ensemble of hard spheres (Boltzman equation[8]). Ogawa et al.[9] suggested that the mechanical energy of granular flow is first transformed into random particle motion and then dissipated. Savage and Jeffrey[10] related this fluctuating velocity to the absolute value of the shear gradient by means of a dimensionless group and observed that the dense phase kinetic theory, as described in the classical book by Chapman and Cowling[8] could be used. In a sheared granular material, the inelasticity of collisions is the only energy dissipation mechanism; otherwise, the particle agitation would increase to infinity due to the input of energy by the shear. In the other limit when $St << 1$, collisions of smooth particles are unlikely as hydrodynamic interactions (lubrication repulsion) prevent actual contacts in a finite time if the roughness or residual Brownian motion are not considered. The rheology

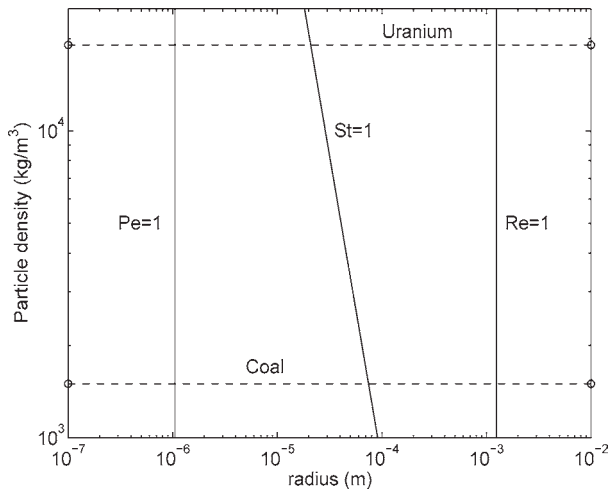

Figure 1. Dependence of the dimensionless numbers on the suspension parameters (a and ρ_p/ρ_f).

Gas considered: air. Solid lines: boundaries for regions where the dimensionless numbers are, respectively, <1 or >1.

and self-diffusion of such suspensions were extensively studied.[11–14]

In the intermediate case, that is, moderate particle inertia, the particles experience a significant drag forcing them to recover the fluid streamlines in a time closely related to the viscous relaxation time scale τ_p. Therefore, three characteristic times control the suspension dynamics: τ_p, τ_f, and τ_c (the typical time spent by a given particle between two consecutive collisions). When the particle inertia is reduced, the role of the drag force is enhanced leading to a significant reduction of the particle kinetic energy. A dynamical equilibrium sets in balancing the energy injected by the shear and the dissipation induced by the drag and the inelastic collisions. The theoretical background of the flow suspension model is based on the conservation equation of the different kinetic stress components. However, solving this problem requires some assumptions and among them the choice of the probability density function of the velocity fluctuations. This input is essential to determine the collisional rate of change of the stress components. Ding and Gidaspow[7] used the Maxwellian velocity distribution function for solving the equations of continuum two-phase flows in a gas–solid fluidized bed, taking into account the drag force effect. For the more fundamental case of sheared flows, the problem was addressed for different flow regimes. In highly agitated suspensions (dry granular flows), Jenkins and Richman[15] have calculated the collisional terms using the deviated Maxwellian function proposed by Grad for homogeneous sheared suspensions.[16] Sangani et al.[17] and Boelle et al.[18] used similar expressions for moderately agitated sytems, taking into account the effect of interstitial fluid. In weakly agitated suspensions, Tsao and Koch[19] proposed a model based on the Dirac function for the velocity distribution function. They obtained a good prediction of the suspension behavior in the limit of dilute and low inertia suspensions. Whereas all these reference studies were concerned with flows at vanishing Reynolds numbers, recent works have investigated the rheology of sheared suspensions in wall-bounded flows in the limit of finite fluid inertia. Kulkarni and Morris[20] analyzed particularly the statistical behavior of noninertial particles using Lattice Boltzmann simulations. Verberg and Koch[21] and Xu et al.[22] have investigated the effect of both the fluid and particle inertia comparing theoretical analysis with Lattice Boltzmann simulations.

This article is devoted to the analysis of sheared suspensions when varying both the particle inertia St and the solid volume fraction ϕ, comparing the behavior of weakly and highly agitated suspensions. The article is organized as follows. First, we summarize the existing statistical theories for flow of suspensions with finite particle inertia. Then, the simulation method is briefly described in the Section on "Simulations". In the next section, the evolution of the particle agitation level, and the kinetic and collisional stresses are commented for different suspension parameters. Only perfectly elastic collisions are first considered, keeping the drag as the only dissipation mechanism. Detailed comparisons of the simulation results with the relevant theories are presented. Then, inelastic collisions are considered in the last section: first a constant restitution coefficient and then a restitution coefficient depending on the impact parameters, which could be a model for local hydrodynamics interactions.

Overview of Existing Theories

The flow of suspensions composed by rigid particles with finite inertia ($St > 1$) and inelasticity ($e \neq 1$) has been addressed theoretically with several assumptions. The theoretical background used to predict the dynamical behavior of these suspensions is briefly described later.

In a linear flow, the velocity field of the unperturbed fluid flow is simply given by

$$\frac{\partial u_i}{\partial x_j} = \gamma_{ij} \tag{1}$$

where $\mathbf{u}$ and $\mathbf{x}$ are, respectively, the fluid velocity and the position vectors. γ_{ij} is the shear rate tensor. For a pure shear flow, $\gamma_{12} = \gamma$ is the only remaining component. The indices 1, 2, and 3 stand, respectively, for the flow direction, for the velocity gradient direction, and for the spanwise direction (or vorticity direction). γ^{-1} is a characteristic time scale of the flow based on the ambient shear. The mean particle motion is equal locally to the fluid flow $\mathbf{U}_p(\mathbf{x}) = \mathbf{u}(\mathbf{x})$

When the particle inertia is finite, the interaction with the fluid (drag force) is significant leading to a reduction of the kinetic energy of the particles. We neglect the effect of gravity, pressure gradient, added mass, and lift forces. The drag is the only force experienced by a particle embedded in the fluid. We consider only the Stokes drag on an isolated particle using Eq. 2. In Eq. 2, $\mathbf{v}$ is the particle velocity and $\tau_p = m_p/6\pi\mu a = St\gamma^{-1}$ the viscous relaxation time of the particle. $\mathbf{u}$ is the local fluid velocity at the particle position. More sophisticate drag correlations were determined taking into account the effects of solid volume fraction and Reynolds number.[6,23–25] However, for our numerical study, Eq. 2 holds in the limit of low to moderate concentrations and negligible Reynolds number. Thus, this simple expression of the drag has been used in the available theories.

$$\frac{d\mathbf{v}}{dt} = -\frac{(\mathbf{v}-\mathbf{u})}{\tau_p} \tag{2}$$

The theory used for dry granular material can be adapted to inertial particles with the additional forcing of the drag.[8] The theoretical model is based on the balance equation for the kinetic stress components, similar to the granular flows, but with additional terms due to drag dissipation. At steady state, the equation for the kinetic stress transport (see Refs. 17 and 18 for more details) becomes in homogeneous configuration:

$$\gamma_{jk}\sigma^k_{ki} + \gamma_{ik}\sigma^k_{kj} + \frac{2}{\tau_p}\sigma^k_{ij} = C_{ij} \tag{3}$$

where C_{ij} is the collisional contribution and $\sigma^k_{ij} = \rho_p \phi T_{ij}$ the kinetic stress tensors. The term $\rho_p\phi$ represents the bulk density. T_{ij} is the velocity fluctuation tensor. For the analytic evaluation of the collisional rate of change of the stress components in Eq. 3, we need an assumption on the particle velocity distribution function $f(\mathbf{c},\mathbf{x})$ and on the two-particle distribution function during a collision $f^{(2)}(\mathbf{c}_A,\mathbf{c}_B)$ (where $\mathbf{c}_A$ and $\mathbf{c}_B$ are the colliding particle velocities). It is assumed that colliding particles are statistically uncorrelated. This is know as the molecular chaos assumption. Similarly to the theory for dense gases,[8] the enhancement of the probability to find close particle pairs for moderate ϕ is accounted by assuming $f^{(2)}(\mathbf{c}_A,\mathbf{c}_B) = g_0 f(\mathbf{c}_A) f(\mathbf{c}_B)$, with g_0 a scalar function that depends on ϕ for a homogeneous suspension. g_0 is given by the peak value of the radial distribution of pairs at contact ($r = 2a$). We use in this paper $g_0 = (1 - \phi/\phi_m)^{-2.5\phi_m}$, proposed by Lun and Savage[26], which tends to infinity when ϕ approaches the close packing volume fraction ($\phi_m = 0.64$) for a random suspension of monodisperse spherical particles.

Solution of highly agitated suspensions

In a high agitation regime of granular flow resulting from a homogeneous shear, Grad[16] proposed to approximate f by a deviated Maxwellian distribution function accounting for a possible anisotropy a_{ij} of the kinetic stress T_{ij} defined by the coefficients:

$$f(\mathbf{c},\mathbf{x}) = \left\{1 + \frac{1}{2}T\, a_{ij}\frac{\partial^2}{\partial c_i \partial c_j}\right\} f_0(\mathbf{c},\mathbf{x}) \tag{4}$$

The components of the kinetic stress tensor T_{ij} are by definition the integral of the second order moments of velocity fluctuations [$nT_{ij} = \int C_i C_j\, f(\mathbf{c},\mathbf{x}) d\mathbf{c}$] over the whole velocity phase space, where $\mathbf{C} = \mathbf{c} - \mathbf{U}_p(\mathbf{x})$ is the local velocity fluctuation relative to the average particulate phase velocity $\mathbf{U}_p(\mathbf{x})$. The particle agitation is calculated from the trace of this tensor $T = T_{ii}/3$. The coefficients a_{ij} are related to the kinetic stress terms according to the following relation:

$$a_{ij} = T_{ij}/T - \delta_{ij} \tag{5}$$

As proposed by Jenkins and Richman,[15] the collisional term can be divided into a source term and a flux term. Eq. 3 becomes:

$$\gamma_{jk}\sigma_{ki} + \gamma_{ik}\sigma_{kj} + \frac{2}{\tau_p}\sigma^k_{ij} = \chi_{ij} \tag{6}$$

where $\sigma_{ij} = \sigma^k_{ij} + \theta_{ij}$ is the total particulate stress tensor and θ_{ij} is the collisional stress tensors. Sangani et al.[17] and Boelle et al.[18] used a similar approach to predict T and T_{ij} for particles of moderate inertia embedded in a viscous fluid in the particular case of a pure shear flow. Finally, the particle agitation in a pure shear flow configuration is solution of an algebraic equation[17]:

$$\sum_{k=0}^{4} d_k \omega_\eta^k = 0 \tag{7}$$

where

$$\omega_\eta = \tfrac{24}{5\sqrt{\pi}}\phi g_0 \eta(2-\eta)\tfrac{\sqrt{T}}{\gamma a}$$
$$d_4 = 15(1-\eta)$$
$$d_3 = (48 - 39\eta)St^{-1}$$
$$d_2 = 3\left[(17 - 11\eta)St^{-2} - \phi^2\alpha\right] - \left(1 + \tfrac{8}{5}\phi\chi\right)\left\{2\eta + 1 - \tfrac{8}{5}\phi\chi(9\eta^3 - 24\eta^2 + 7\eta + 5)\right\}$$
$$d_1 = 3(2-\eta)St^{-1}\left[3St^{-2} - 2\alpha\phi^2 + \tfrac{4}{5}\phi\chi\left(1+\tfrac{8}{5}\phi\chi\right)(1-\eta)(3\eta+1)\right]$$
$$d_0 = -3\alpha\phi^2 St^{-2}(2-\eta)$$

and $\alpha = \frac{384}{25\pi} g_0^2 \eta^2 (2-\eta)$ and $\eta = (1+e)/2$. Equation 7 is valid for elastic and inelastic collisions indicating that once the shear is imposed to the suspension, the dimensionless granular temperature $T/\gamma^2 a^2$ is a function of the suspension characteristics (Stokes number, concentration, and restitution coefficient).

The coefficients a_{ij} depend only on the suspension characteristics (St, ϕ, and e). Inserting Eq. 5 in Eq. 6 leads to the following expressions for the anisotropic coefficients (see Ref. 17):

$$a_{22} = a_{33} = -\frac{a_{11}}{2} = -\frac{5(1-\eta)\omega_\eta + 3(2-\eta)St^{-1}}{3(2-\eta)\left(\omega_\eta + St^{-1}\right)} \tag{8a}$$

$$a_{12} = \frac{1}{2\left(\omega_\eta + St^{-1}\right)} \times \left\{-\left(1 + \frac{8}{5}\phi g_0 \eta\right)a_{22} - (1 + 4\phi g_0\eta) + \frac{12}{5}\phi g_0 \eta(2-2\eta)\right\} \tag{8b}$$

Solution for dense flow and high solid phase intertia

In a dense flow and at large Stokes number, the effect of hydrodynamic interactions among particles is small and the particles travel in nearly straight lines between successive collisions. Thus, the particles are expected to behave similarly to the molecules of a dense gas consisting of smooth, spherical molecules with a hard-sphere interaction potential. Therefore, as proposed by Sangani et al.,[17] the standard expressions for the equation of state, viscosity, and conductivity of dense granular materials can be used. Moreover the particle velocity distribution is close to an isotropic Maxwellian so this one can be used to estimate the leading-order of the energy dissipated due to inelastic collisions. The velocity variance is determined by equating the energy input in shearing the suspension to the energy dissipation by inelastic collisions and viscous effects. This lead to the following expression Eq. 9:

$$\left(\frac{\sqrt{T}}{\gamma a}\right)^2 = \frac{4}{15(1-e)}\left[1 + \frac{\pi}{12}\left(1 + \frac{5}{8\phi g_0}\right)^2\right] \tag{9}$$

For perfectly elastic particles ($e = 1$) and high but finite Stokes number, T is given by

$$\frac{\sqrt{T}}{\gamma a} = \frac{16}{15\sqrt{\pi}} St\phi g_0 \left[1 + \frac{\pi}{12}\left(1 + \frac{5}{8\phi g_0}\right)^2\right] \tag{10}$$

Solution of weakly agitated suspensions

When both the suspension concentration and the particle inertia are low, the relaxation time of the particle τ_p is of the same order or lower than the average time between successive collisions τ_c. Particles have very weak velocity fluctuations as they more likely recover the fluid streamlines after a collision. This peculiar regime was called by Tsao and Koch "the quenched state" as opposed to the "ignited theory" for agitated systems. Tsao and Koch[19] proposed to close the equations assuming a Dirac function [$f(C) = \delta(C)$] for the velocity distribution function. It means that all the particles are moving with the local fluid velocity and that collisions are only shear-induced. However, their formulation holds only for dilute particulate flows since they considered that the two-particle distribution function in the collisional terms verifies $f^{(2)}(\mathbf{c}_A, \mathbf{c}_B) = f(\mathbf{c}_A)f(\mathbf{c}_B)$ ($\mathbf{c}_A$ and $\mathbf{c}_B$ are the colliding particle velocities). For moderate ϕ, the enhancement of the probability to find close particle pairs could be accounted for, similarly to the theory for dense gases,[8] by assuming $f^{(2)}(\mathbf{c}_A, \mathbf{c}_B) = g_0 f(\mathbf{c}_A)f(\mathbf{c}_B)$. A verification of Tsao and Koch's approach permitted us to point out that a factor 2 is missing in the collision terms (Eqs. 4.8 and 4.9 of Ref. 19). The kinetic stress terms are obtained by solving the Eq. 3 and leads to the following relations for $e = 1$:

$$\frac{T_{11}}{(\gamma a)^2} = 2g_0 \frac{64}{315\pi} St^3\phi \left[1 + \frac{9\pi}{16}\frac{1}{St} + \frac{2}{St^2}\right] \tag{11a}$$

$$\frac{T_{22}}{(\gamma a)^2} = 4\frac{T_{33}}{(\gamma a)^2} = 2g_0 \frac{128}{315\pi} St\phi \tag{11b}$$

$$\frac{T_{12}}{(\gamma a)^2} = -2g_0 \frac{64}{315\pi} St^2\phi \left[1 + \frac{9\pi}{16}\frac{1}{St}\right] \tag{11c}$$

By summation of the diagonal terms, $T = T_{ii}/3$:

$$\frac{T}{(\gamma a)^2} = 2g_0 \left(\frac{64}{945\pi} St^3\phi \left[1 + \frac{9\pi}{16} St^{-1} + \frac{9}{2} St^{-2}\right]\right) \tag{12}$$

The theoretical collisional stress components are null in the quenched regime.

Modelling the multibody hydrodynamic interactions

In moderately concentrated to dense suspensions, the multibody hydrodynamic interactions can be a major phenomenon that controls the level of particle agitation in suspension. Sangani et al.[17] modeled these interactions by a corrective function $R_{diss}(\phi)$ applied to the Stokes drag. Using this correction prefactor yields a reduction of the overall Stokes number of the suspension flow. Wylie et al.[27] included in the coefficient R_{diss} the effect of finite fluid inertia in the limit of infinite particle inertia. Later, Verberg and Koch[21] studied sheared suspensions with finite inertia of the fluid and tested the validity of their theory in the limit of finite Stokes numbers. We neglect the effect of the multibody hydrodynamic interactions in the simulations where the restitution coefficient is constant. However, in the section "Restitution coefficient including hydrodynamic effects", the effect of binary hydrodynamic interactions is modeled with an alternative approach: an effective restitution coefficient is estimated for each collision between two particles based on the impact parameters.

Simulations

For investigating the suspension dynamics and testing the accuracy of the theoretical predictions when the particle inertia is finite, we carried out discrete particle simulations, where we assume that the fluid flow is not perturbed by the presence of the particles. The particles are considered as hard spheres. They experience only Stokes drag force and binary collisions which is valid for low to moderate solid concentration. A fixed time step dt is used for time integration of the trajectories using a fourth order Adams-Bashforth scheme. Particles are initially seeded at nonoverlapping random positions within the entire domain and their velocity is set to the local fluid velocity ($u_1 = \gamma x_2$) (γ being the shear rate). The detection of a collision occurs when the distance between two particle centers is less or equal to their diameter ($|\mathbf{x}_A - \mathbf{x}_B| \leq 2a$). Actually, our numerical scheme is close to the classical hard-sphere model. We did not select an event-driven scheme but rather used a small constant time step dt. After the end of the new time step, overlapping particles are detected and the exact collision time of each collision ($t + \delta t_i$, where $\delta t < dt$) is precisely determined between t and $t + dt$. The postcollision velocities are calculated and each particle is moved forward in time from $t + \delta t_i$ to $t + dt$. The numerical scheme is illustrated in Figure 2.

The simulations are performed in a cubic domain of width $L = 2\pi$. The particle size is kept constant ($L/a \approx 48$) and various volumetric concentrations of the suspension are investigated when varying the total number of particles. Periodic boundary conditions in the three directions of space help preserving the homogeneity of the suspension under shear. When a particle exits the simulation domain from the bottom (resp. upper) boundary, it appears on the opposite side and its velocity is adapted by adding (resp. subtracting) the local flow velocity γL. This is equivalent to applying the shear in a dynamic way by means of the Lees-Edward boundary conditions.[28] The ratio L/a has been selected fitting the two following constraints: not too large for preventing the formation of layers populated with particles[29] and not too small so that each particle may encounters many collisions when travelling between two opposite boundaries.

The time step has to be carefully selected. We strictly verified the condition $dt = \min(\tau_p, \tau_c)/50$ for all the simulations. This condition meets the two following requirements: each particle trajectory recovering the fluid streamline on the time scale τ_p is well-resolved and for highly inertial particles the time spent between two consecutive collisions τ_c is discretized in at least 50 time steps. The collision time scale is calculated a priori using the theoretical analysis described in

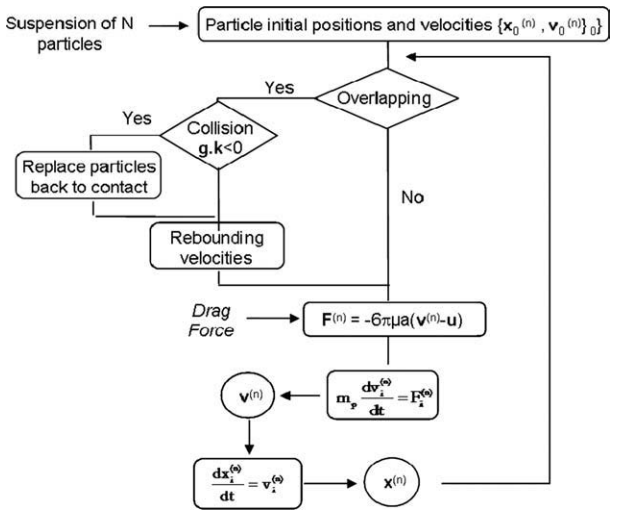

Figure 2. Sketch of the numerical scheme at time step *n*.

the previous section assuming that the suspension is strongly agitated:

$$\tau_c = \frac{a\sqrt{\pi}}{12\phi g_0 \sqrt{T}} \tag{13}$$

The level of particle agitation T in Eq. 13 is estimated using Eq. 7 once the Stokes number, the volumetric concentration, and the restitution coefficient are fixed. There is no numerical limitation on the relaxation time τ_p when the particles are highly inertial but attention should be paid in the simulations with low Stokes numbers for preventing successive collisions (see Ref. 30). The selection of the time step in a very dilute suspension needs even more care as two additional conditions should be satisfied. First, the time step has to be much smaller than a time scale based on the velocity fluctuation $a/\sqrt{T}$, especially at high particle inertia. Second, a particle must experience several collisions as it travels through the entire domain of simulation. The condition $\tau_c << L/\sqrt{T}$ prevents an unrealistic increase of the suspension agitation energy due to the accumulation of $L\gamma$ velocity increments (or decrements) when particles are crossing the bottom (resp. upper) boundary conditions many times without experiencing collisions.

The particle radius a and the shear rate γ^{-1} are used, respectively, as length and time scales for normalizing all the statistical quantities. The average over particles are formed every 10 time steps. After the initial seeding, all the statistics evolve along a transient regime which is not considered in the analysis. Then, the flow of the suspension is simulated during a time long enough to guarantee the convergence of the statistics. The most critical constraint was observed on the length of time series required to reach a diffusive behavior for the dispersion of particles.[13,31] Typically, each particle was allowed to experience at least 600 collisions. This typical number of collisions is only indicative and varies strongly with the concentration and the Stokes number. The selection of the simulation time to achieve statistical convergence is not made a priori. Actually, the simulations were run until the particle flow statistics (particle agitation, stress terms, self-diffusion…) have reached a steady-state.

Statistical Quantities for Elastic Collisions and Varying Particle Inertia

Based on the two versions of the theory described previously, we expect distinct responses of the flow suspension for different characteristics (St and ϕ). In the present section, we investigate the influence of the drag as the only dissipative mechanism (perfectly elastic collisions) on the macroscopic behavior of the suspension when varying the Stokes number. Two asymptotic cases can be identified. When $St >> 1$, the particle fluctuating energy is high. Thus, Tsao and Koch[19] have shown that for $St > 5$ the suspension is always highly agitated even for low concentration. When $St << 1$, the energy of particle fluctuations is very low, short distance interactions are dominant and the role of hydrodynamic interactions[11,13,14] and lubrication are the major effects. Therefore, we restrict our simulations to moderate particle inertia ($1 \leq St \leq 10$). This range of parameters has shown extremely rich dynamics for dilute suspensions[17] and we aim at simulating low to moderate concentration ($5\% \leq \phi \leq 30\%$).

Particle agitation

The level of particle velocity fluctuations is measured by $T = T_{ii}/3$, where T_{ij} is given by Eq. 14 where $\langle\rangle$ is an average formed over all the particles and over the simulation time (the initial transient time to reach a statistical equilibrium is not considered).

$$T_{ij} = \left\langle v_i'' v_j'' \right\rangle - \left\langle v_i'' \right\rangle \left\langle v_j'' \right\rangle \tag{14}$$

$\mathbf{v}''$ is equivalent to the variable $\mathbf{c}$ in the phase space, and it corresponds to the particle velocity fluctuation relative to the ensemble average velocity $\mathbf{U}_p(\mathbf{x}) = \gamma x_2 \mathbf{i}_1$. We have verified that the velocity fluctuation averages $\left\langle v_i'' \right\rangle \left\langle v_i'' \right\rangle$ are negligibly small compared with $\left\langle v_i'' v_j'' \right\rangle$ (typically $\left\langle v_i'' \right\rangle \left\langle v_i'' \right\rangle / \left\langle v_i'' v_j'' \right\rangle < 10^{-4}$). In the limit of high Stokes numbers, the simulations for high concentrations have to be carefully carried out. A very short time step $O(10^{-4}\gamma^{-1})$ is required due to the high collision frequency to resolve all the collisions. Instantaneous multiple collisions are not considered in the numerical model and this can lead to short time overlapping of the particles.

Figure 3 shows the numerical results of the particle agitation when varying the concentration for different Stokes numbers. When increasing St from 1 to 10 for a given ϕ, the agitation level is enhanced by three orders of magnitude. In the limit of high St, two distinct trends are observed at low and high solid fractions. In dilute suspensions, the particle agitation decreases with the concentration because of the reduction of the interparticle distance. In dense suspensions, the particle agitation level remains high although the mean free path of the particles is reduced. For small St, the particle agitation increases monotonically with the concentration.

For moderate to high St numbers ($St = 5 - 10$), the level of particle agitation obtained by the simulations or predicted

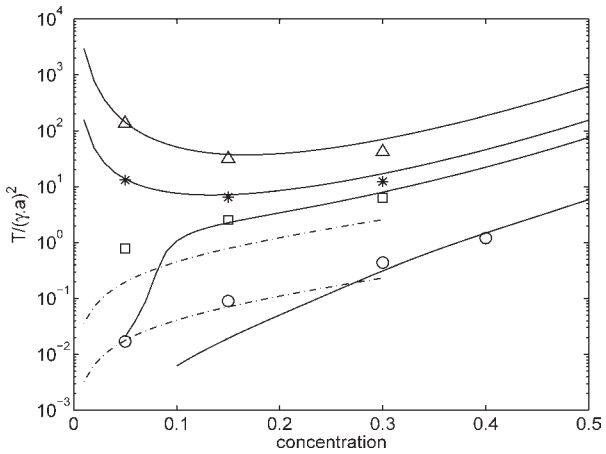

Figure 3. Particle agitation vs. the solid volume fraction for different Stokes numbers (from. Ref. 31). Symbols (Δ, *, □, and ○ are, respectively, for *St* = 10, 5, 3.5, and 1) represent the numerical results.

Solid lines (from top to bottom $St = 10$, 5, 3.5, and 1) correspond to the theoretical predictions of Eq. 7. Dashed-dotted line (from top to bottom $St = 3.5$ and 1) correspond to the quenched theory prediction Eq. 12.

by the kinetic theory for the ignited state match very well. Moreover, we verified that for $St = 10$ the simplified expression (Eq. 10) valid for $St \to \infty$ is also a very good estimate. Therefore, we do not expect new features for St higher than 10. In contrast, for lower Stokes numbers the theoretical prediction using the ignited state is far from being accurate at low concentrations (two orders of magnitude discrepancy when $\phi = 5\%$). Figure 3 shows clearly that the theory (Eq. 7) is only valid for strongly agitated suspensions ($T > \gamma^2 a^2$, the so-called ignited state). A transition (depending on St and ϕ) exists. Below this limit, the suspension agitation is weak but finite (so-called quenched state). Similar results have been obtained in Boelle et al.[18] for lower Stokes numbers ($St = 0.5$).

The underestimation of T by the theory for moderately inertial particles at low St and ϕ is presumably a direct consequence from the assumptions used to derive Eq. 7. Indeed, a major input for this theoretical prediction is the expression of the probability density function of velocity fluctuations. It is assumed to be a deviated Maxwellian function. The analysis of the velocity distribution function obtained in the simulation is crucial to validate such an hypothesis. At high St, we verified that for each case, $f(v_i'')$ has the shape of a Gaussian function or equivalently $f(\mathbf{v}'')$ is close to a Maxwellian function. It is not the case at low ϕ and St. For instance at $St = 1$, the velocity distribution function shown in Figure 4 experiences a dramatic evolution when ϕ is varied. It is close to the Gaussian distribution at $\phi = 30\%$ but the velocity distribution is highly peaked around $v_1'' = 0$ for dilute suspensions ($\phi = 5\%$) (similar observation for v_2'' and v_3''). It indicates that most of the particles are following the fluid streamlines with weak velocity fluctuation. The simulations showed that when the solid volume fraction is reduced, the occurence of low velocity fluctuations is strongly enhanced. Hence, the total number of particles with zero velocity fluctuations is increased (quenched state). This flowing regime is dominated by the drag.

In the limit of high inertia, the particles fly randomly following straight paths (only weak damping of the velocity by the drag between two consecutive collisions). Such a flow regime is collision-dominated where most collisions are driven by the fluctuating energy of the particles (ignited state). In contrast, for the quenched state most collisions are shear-induced. We showed in Ref. 31 that the time scale ratio τ_p/τ_c (particulate relaxation time compared with the typical time between successive collisions) indicates the transition from the drag to the collision dominated regime. The dominant mechanism has the smallest time scale. τ_p is imposed in the simulations by the selection of the Stokes number, whereas τ_c is calculated using the collision frequency computed from the total number of collisions detected during a certain simulation time. For the two regimes, τ_c can be estimated. In simulations where the agitation is high, Eq. 13 is accurate whereas Eq. 15 is more adequate for shear driven collisions. The transition between the ignited and the quenched state occurs when $\tau_p/\tau_c = O(1)$.

$$\tau_{c\gamma} = \frac{\pi}{16\phi\gamma} \tag{15}$$

Both the analysis of the collision time scale and the shape of the velocity distribution function suggest that at low concentration and low Stokes numbers the suspension is flowing in the quenched regime. Then, the results of the simulation in the Figure 3 have to be compared with the prediction of Eq. 12. It is clear that the prediction based on the quenched theory is much closer to the simulation results than the ignited regime assumption (especially for $St = 1$ and $\phi = 5\%$ or 15%). The remaining discrepancy between the simulations and the quenched theory may be inferred to the underestimation of the collisional change in the stress tensor. Indeed, the quenched theory considers only the shear-

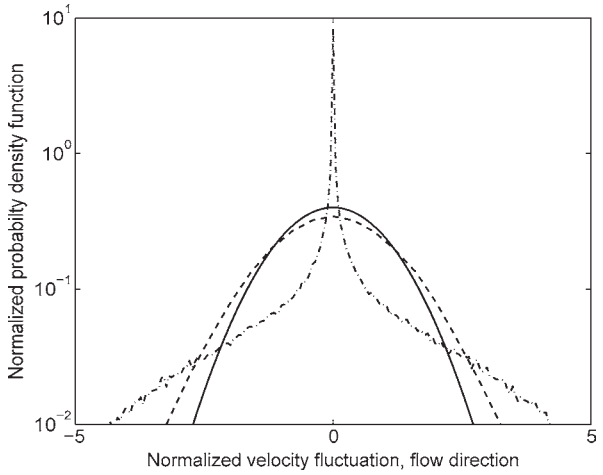

Figure 4. Normalized probability density functions vs. normalized velocity fluctuations in the flow direction $\left(v_1/\sqrt{(T)}\right)$ for ϕ = 5%.

Dashed-dotted and dashed lines correspond, respectively, to $St = 1$ and 5. Solid line: Gaussian distribution function.

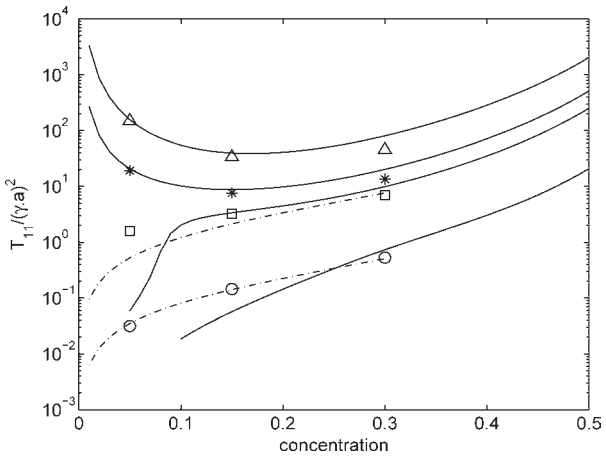

Figure 5. Kinetic stress component in the flow direction $T_{11}/(\gamma a)^2$ vs. the solid volume fraction for different Stokes numbers.

For caption see Figure 3.

induced collisions and neglects the existence of the additional collisions driven by the agitation. These events are not frequent but contribute to keep a higher level of agitation for $St = 3.5$ and $\phi = 5\%$.

Stress tensor of the particulate phase

Normal Components. Momentum transfer in the suspension is characterized by stress tensors and we can gain insightful information on the physics by analyzing the different contributions. In a suspension of solid particles, there are two distinct contributions: the kinetic part ($\rho_p \phi T_{ij}$) where the momentum is carried by moving particles and the collisional part θ_{ij} which corresponds to transfer by the collisions. The total dimensionless stress tensor is hence:

$$\sigma^*_{ij} = \frac{1}{\rho_p \phi \gamma^2 a^2}\left(\rho_p \phi T_{ij} + \theta_{ij}\right). \tag{16}$$

We first discussed the diagonal terms of these tensors. The stress tensor components were computed for the same simulation sets presented ($St \in [1 - 10]$, $\phi \in [5 - 30\%]$ and $e = 1$). The evolution of the kinetic stress component T_{11} is shown in Figure 5 for different St and ϕ. The other normal components (T_{22} and T_{33}) are not shown but behave similarly. Depending on the flowing regime, the numerical results are compared with the relevant theory. The kinetic stress components increase monotonically with the concentration in the limit of low Stokes numbers, whereas they show a local minimum in the limit of high inertia (for $\phi \approx 15\%$). For a dilute and highly inertial suspension, the kinetic stress is dominating over the collisional contribution as the particles may travel relatively long distances between collisions. However, in concentrated suspensions, the collision frequency increases sharply and collision-induced momentum transfer becomes important.

The theoretical expression for the collisional stress is obtained by integrating the momentum transfer over all the collisions.[15]

$$\theta_{ij} = (1+e)\rho_p \phi^2 g_0 \left\{ \left(2T - \frac{8}{5} a \sqrt{\frac{T}{\pi}} e_{kk} \right) \delta_{ij} + \frac{4}{5}\left(T_{ij} - T\delta_{ij}\right) - \frac{16}{5} a \sqrt{\frac{T}{\pi}} e_{ij} \right\} \tag{17}$$

where $e_{ij} = (\gamma_{ij} + \gamma_{ji})/2$. The collisional stress tensor components are calculated explicitly in the simulations using the impulse difference $\mathbf{j} = m_p(\mathbf{v}' - \mathbf{v})$ occurring at each collision. The volumetric collisional stress averaged over the simulation time T_{sim} is given by

$$\theta_{ij} = \frac{2a}{\vartheta T_{sim}} \sum_{coll} m_p \left(j_i k_j\right) \tag{18}$$

where $\vartheta = (2\pi)^3$ is the total volume of the domain. Particles involved in a collision have to verify $\mathbf{g.k} < 0$ at contact.

The numerical results for the collisional stress component θ_{11} are compared to Eq. 17 in Figure 6. In contrast to the kinetic stress, the collisional stress components always increase with concentration because of the increasing collision frequency. Although the kinetic stress is dominant in dilute and highly inertial suspensions, the collisional contribution becomes significant and may even dominate in more concentrated suspensions where momentum and energy transfers are related to collisions ($\frac{\theta_{ij}}{\rho_p \phi T_{ij}} > 2$, see Figures 5 and 6).

The shear flow forces a stress anisotropy in the solid-phase (difference in the normal stresses). The stress redistribution χ_{ij} between the different components contains the contribution of collisions which leads generally to a reduction of anisotropy. Indeed, when the restitution coefficient $e = 1$, the collisions do not dissipate energy but mainly transfer momentum in the suspension over the different directions. Equation 19 shows that when $e = 1$ and $\gamma = 0$ (elastic collisions in a quiescent fluid), the collisional momentum transfer is not zero as long as the particle agitation is finite and the kinetic stress tensor is anisotropic. This will lead to the redistribution of the kinetic energy of the suspension.

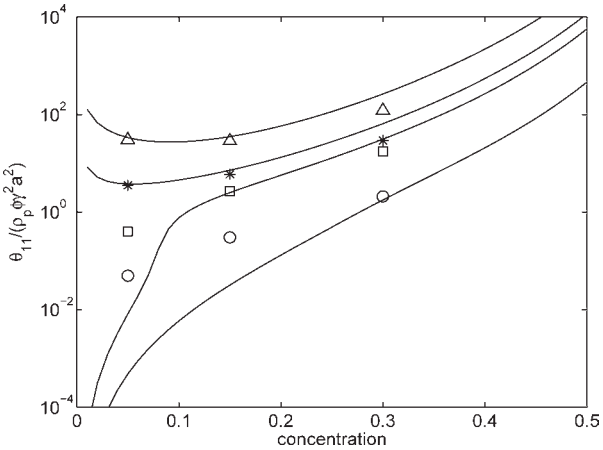

Figure 6. Collisional stress component in the flow direction $\theta_{11}/(\rho_p \phi \gamma^2 a^2)$ vs. the solid volume fraction for different Stokes numbers.

For caption see Figure 3.

$$\chi_{ij} = (1+e)\rho_p \phi^2 g_0 \left\{ \left[\frac{2}{3}\frac{(e-1)}{\phi g_0}\frac{T}{\tau_c} - \frac{2}{5}(3e-1)Te_{kk} \right]\delta_{ij} \right\} + \frac{1}{5}\frac{(3-e)}{\phi g_0}\frac{T_{ij}-T\delta_{ij}}{\tau_c} + \frac{12}{5}(2-e)Te_{ij} \quad (19)$$

The stress in the suspension of moderately inertial particles does not develop equally in all the directions. The kinetic stress in the flow direction is always dominant because it is directly produced by the mean shear of the flow. The other diagonal terms of the kinetic stress arise only from the collision contribution as there is no production by the shear rate in those directions. They are essentially induced by the redistribution due to collisions (through χ_{22} and χ_{33}). For a fixed Stokes number, when the concentration increases the influence of the collisional momentum transfer overcomes the drag contribution [Eq. 3]. The redistribution of the fluctuating energy is enhanced and the difference between the diagonal component of the kinetic stress tensor decreases (see the coefficients a_{ij} in Figures 7a,b). Consequently, the flow of the suspension tends to recover a Newtonian behavior.

At high particle inertia or concentration, the anisotropy is weak. The agreement between the simulations and theory is very good for $St = 5$, where the drag contribution to each kinetic stress component is moderate. The kinetic stress is quasi-isotropic when ϕ approaches 30%. All the results on the anisotropy can be interpreted in terms of the ratio of the two significant time scales τ_p/τ_c.[31]

Off-Diagonal Components: Viscosity of the Particulate Phase. Because of symetry, only two off-diagonal terms of the stress tensors are non-zero: T_{12} and θ_{12}. Their behavior is similar to the respective normal stress components when the Stokes numbers and concentration are varied. Kinetic shear stress is dominant at low ϕ and high St whereas the collisional contribution dominates at high ϕ. The agreement is also good with the appropriate theoretical prediction (ignited or quenched regime).

The effective viscosity of the solid phase can be calculated from the two shear stress components. The kinetic contribution to momentum transfer can be interpreted as a kinetic viscosity. Rearranging T_{12} (Eq. 8b), the expression of the kinetic viscosity $\mu_s^{kin} = -\rho_p \phi T_{12}/\gamma$ can be written in terms of the different time scales and the anisotropy coefficient as follows:

$$\frac{\mu_s^{kin}}{\rho_p \phi \gamma a^2} = \frac{T}{\gamma^2 a^2}\left(\frac{2}{\gamma\tau_p} + \frac{\sigma_c}{\gamma\tau_c}\right)^{-1}\left\{(1+\phi g_0 \phi_c) - \frac{a_{11}}{2}\left(1+\frac{8}{5}\phi g_0 \eta\right)\right\} \quad (20)$$

where $\phi_c = \frac{2}{5}(1+e)(3e-1)$ and $\sigma_c = \frac{1}{5}(1+e)(3-e)$.

Similarly, the collisional particulate viscosity $\mu_s^{coll} = -\theta_{12}/\gamma$ comes from the collisional shear stress component θ_{12} and is given by:

$$\frac{\mu_s^{coll}}{\rho_p \phi \gamma a^2} = \frac{8}{5}\phi g_0 (1+e)\left(\frac{\mu_s^{kin}}{\rho_p \phi \gamma a^2} + \frac{2}{\sqrt{\pi}}\frac{\sqrt{T}}{\gamma a}\right) \quad (21)$$

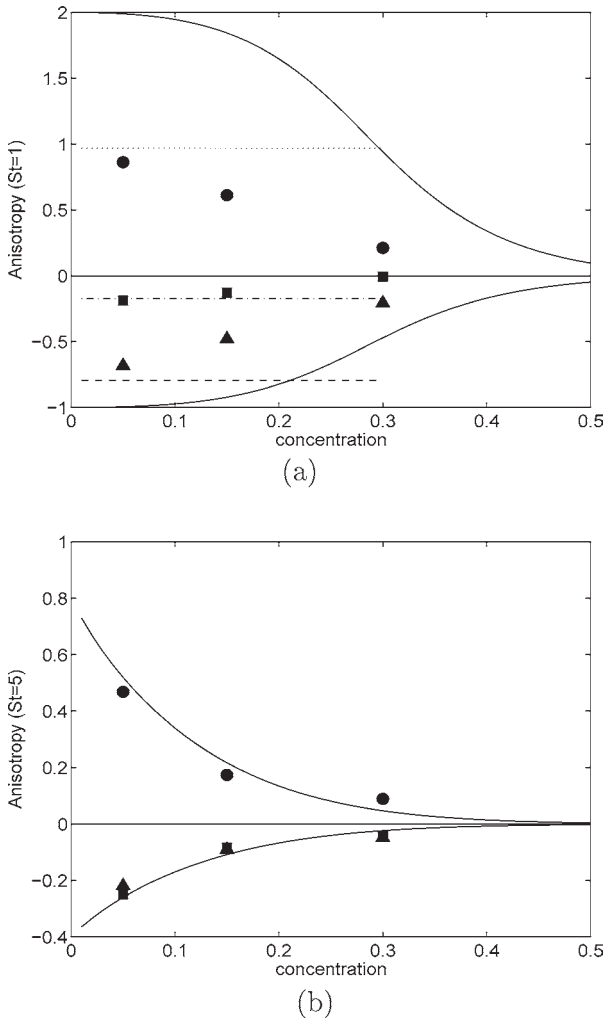

Figure 7. The diagonal terms of the tensor a_{ij} vs. the solid volume fractions.

Figure a) is for $St = 1$ and figure b) for $St = 5$. Symbols: numerical results (●, ▲, and ■ are, respectively, for the flow, shear, and spanwise directions). Solid lines: theoretical predictions [Eqs. (8a)] of highly agitated suspensions (the positive line is for a_{11} and the negative lines for a_{22} and a_{33}). The dotted, dashed, and dotted-dashed lines correspond, respectively, to the flow, shear, and spanwise directions predicted by the quenched theory [Eqs. (11a) to (11c)] for weakly agitated suspensions.

Finally, the total suspension viscosity may be deduced by summing both the kinetic and collisional contributions:

$$\mu_s = \mu_s^{kin} + \mu_s^{coll} \quad (22)$$

Based on similar assumptions, a simplified model for the effective viscosity has been proposed by Balzer et al.[32] to carry out Eulerian simulations of dense fluidized beds.[33] Using the so-called Boussinesq assumption $T_{ij} = T\delta_{ij} - \mu_s^{kin}\gamma_{ij}$, their model (Eq. 23) considers that the normal stress components are equal and that the anisotropic part of the kinetic stress tensor is proportional to the shear rate. It is clear from Figure 8 that the simplified model predicts accurately the simulation results in the highly agitated regime where the collisions are driving the flow and the anisotropy is weak. In these situations, the additional term a_{11} included in Eq. 20 may be omitted.

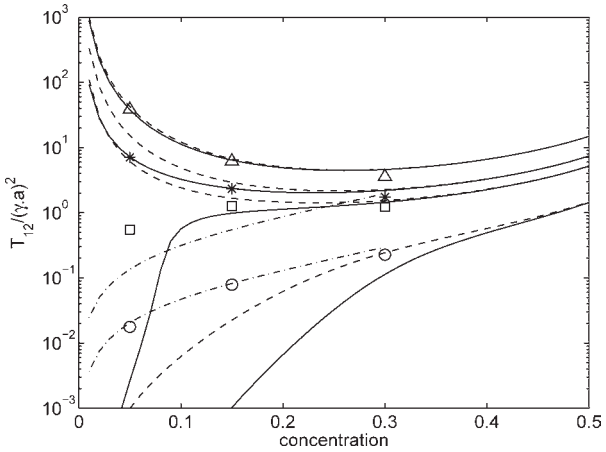

Figure 8. Comparison between the particulate kinetic viscosity $|T_{12}|/(\gamma a)^2$ obtained by solving the complete kinetic stress transport equations (solid lines) and the kinetic viscosity obtained by the model with the Boussinesq assumption (dashed lines).

The prediction of the quenched theory is also represented via the dotted-dashed lines. Symbols refer to the same Stokes numbers as in Figure 3.

$$\frac{\mu_{\mathrm{mod}}^{\mathrm{kin}}}{\rho_{\mathrm{p}}\phi\gamma a^2} = \frac{T}{\gamma^2 a^2}\left(\frac{2}{\gamma\tau_{\mathrm{p}}} + \frac{\sigma_{\mathrm{c}}}{\gamma\tau_{\mathrm{c}}}\right)^{-1}(1 + \phi g_0 \phi_{\mathrm{c}}) \qquad (23)$$

Equations 20 and 21 indicate that both the kinetic and collisional contributions to the viscosity do not depend directly on the magnitude of the shear rate, but indirectly through the particle agitation generated by particle encounters. The weight of each contribution evolves with concentration. In dilute regimes, the kinetic viscosity is very high because momentum transfer occurs due to high fluctuation energy of the particles. The role of collisions appears in both contributions through the product ϕg_0 which increases sharply for dense suspensions. Figure 9 shows the evolution of the total particulate viscosity. We can see that in dense suspensions, the kinetic viscosity alone is far from predicting the total suspension viscosity as the contribution of the collisions becomes dominant at high concentration. We note that the trend at low concentration is very different for ignited or quenched suspensions.

Effect of the Restitution Coefficient

In the previous section, we discussed the macroscopic behavior of suspensions, where the drag is the only mechanism of energy dissipation. Actually, other physical mechanisms of dissipation may exist: local hydrodynamic interactions (and possibly multibody for dense suspensions), film drainage during a collision event, short-range surface forces, and inelastic deformation of the particles. All these phenomena will modify the energy budget and may induce a significant reduction of the particle agitation. According to Wylie et al.,[27] the viscous dissipation is dominant on the inelasticity effect in liquid–solid suspension rather than in gas–solid suspensions for low to moderately concentrated suspensions. However, the viscous dissipation can be dominant in gas–solid suspensions at high solid volume fractions.

In configurations where the viscous dissipation may be neglected, the influence of the inelasticity effect on the macroscopic behavior of an agitated granular material (without drag) was investigated in many works.[34,35] A restitution coefficient lower than 1 (even slightly, $(1 - e) << 1$) reduces considerably the agitation level of the suspension. In a dry granular material where the drag force is neglected, the dissipation due to inelastic effects is the only dissipative mechanism. Therefore, the equilibrium state is achieved under the balance of shear induced agitation due to collisions and inelastic dissipation. When the collision inelasticity is supplemented by a second energy dissipation mechanism, the agitation level in the suspension is even lower.

In addition to the drag and collision dissipation mechanisms, Sangani et al.[17] took into account the local hydrodynamic interactions in the energy conservation equation in the limit of vanishing Reynolds number and moderate to high Stokes number. The authors showed that the effect of hydrodynamic interactions can be simply modeled by a corrective function $R_{\mathrm{diss}}(\phi)$ applied to the Stokes drag on each particle trajectory. They compared favorably this model with simulations accounting for hydrodynamic interactions through the Stokesian Dynamics approach. Using this correction, prefactor is similar to a reduction of the overall Stokes number of the suspension flow.

In this section, we aim at investigating the respective influence of inelastic collisions, lubrication effects, Stokes drag, and solid volume fraction on the behavior of the suspension. First, the case of constant restitution coefficient is considered. This coefficient is generally related to the loss of energy due to the surface contact. Second, we introduce a model for including the lubrication effects in a restitution coefficient based on the correlation of Ref. 36. In all cases, the existence and the range of parameters leading to quenched or ignited state will be compared with the reference case of perfectly elastic particles.

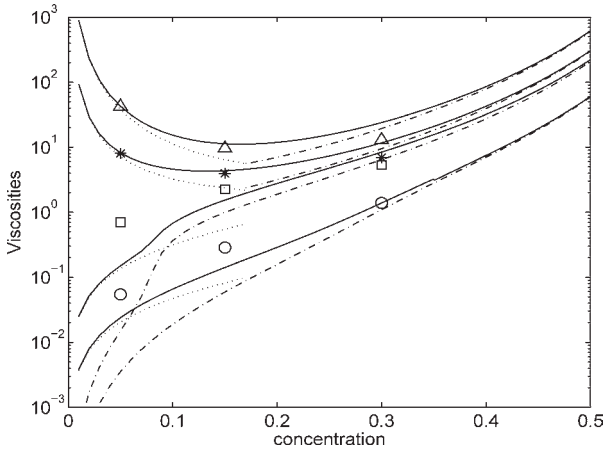

Figure 9. Total viscosities $\mu_{\mathrm{s}}/(\rho_{\mathrm{p}}\phi\gamma a^2)$ vs. concentration.

The solid lines and the symbols are for the total viscosity (they refer to the same Stokes numbers as Figure 3). The dotted and dotted-dashed lines are, respectively, for the kinetic $\mu_{\mathrm{s}}^{\mathrm{kin}}/(\rho_{\mathrm{p}}\phi\gamma a^2)$ and collisional $\mu_{\mathrm{s}}^{\mathrm{coll}}/(\rho_{\mathrm{p}}\phi\gamma a^2)$ viscosities of the particulate phase.

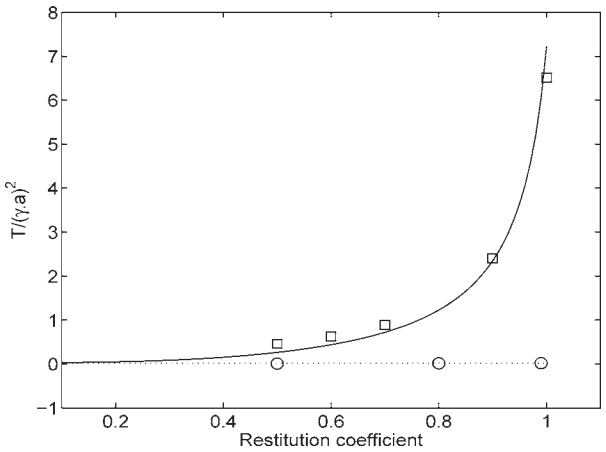

Figure 10. Particle agitation $T/(\gamma a)^2$ vs. the restitution coefficient.

Circles and dotted line: simulations and quenched theory for the case $St = 1$ and $\phi = 5\%$. Squares and solid line: simulations and ignited theory for $St = 5$ and $\phi = 15\%$.

Constant restitution coefficient

We carried out some simulations combining finite drag and inelastic collisions (with constant restitution coefficient) by decreasing the restitution coefficient for fixed St and ϕ. At $St = 5$ and $\phi = 15\%$, the flow regime of the suspension is ignited for perfectly elastic collisions. When the restitution coefficient varies from 1 to 0.5, the particle agitation decreases roughly by an order of magnitude (see Figure 10). We observed that the velocity distribution is still very close to a Maxwellian function. The anistropy of the suspension is more pronounced as the effect of inelastic collisions is increased (see Figure 11). In the case of a suspension with $St = 1$ and $\phi = 15\%$, the velocity variance is almost independent of the collision inelasticity and is fairly well-predicted by the theory using the quenched state with $e = 1$. We can conclude that highly agitated suspensions are very sensitive to the inelasticity of collisions whereas suspensions flowing under the quenched regime are almost unaffected by the value of the restitution because collisions events are less frequent.

The dissipation of kinetic energy during a single binary collision between two particles A and B is: $\Delta E = -\frac{1}{4}(1-e^2)(v_A - v_B)^2$. The global energy dissipation due to inelasticity over the whole suspension can be calculated from $(\chi(mc^2) = \chi_{ii} = -(1-e^2)\rho_p \phi \frac{T}{\tau_c})$ which corresponds to the average energy loss for each collision multiplied by the collision frequency. Including the effect of drag, the ratio $(\tau_p/\tau_c)(1-e^2)/2$ compares the typical rate of energy dissipation due to the drag $1/\tau_p$ to the energy loss during inelastic collisions $((1-e^2)/2\tau_c)$.

Figure 12 shows the evolution of the particle agitation for $St = 5$ as a function of $(\tau_p/\tau_c)(1-e^2)/2$ which is the dissipation ratio between collision and drag effects. The collision time is evaluated using Eq. 13 where T is the real particle agitation obtained in the simulations. The numerical results are compared with the prediction of the theory based on an ignited state. The shape of this curve is not intuitive because τ_c varies with the particle agitation leading to a nonmonotonic evolution of the dissipation ratio when the restitution coefficient decreases. The simulation results and the theory agree well for $e > 0.9$. The dominant contribution to the dissipation is due to the drag while $(\tau_p/\tau_c)(1-e^2)/2$ is less than 1. For $e < 0.9$, the dissipation related to all the inelastic particle collisions becomes dominant. The dissipation ratio starts to decrease for $e < 0.6$, indicating that although the ignited theory is still valid, the drag overcomes the dissipation by inelastic collisions at low particle agitation.

The discrepancy observed in Figure 12 between the theory and the simulations at low restitution coefficients is related to the poor prediction of the ignited theory for weakly agitated systems. In those cases of low restitution coefficients, we observe frequent particle clustering. This phenomenon has been often observed in sheared inelastic granular materials. The clusters show a preferential orientation along the compression axis of the flow along which shear-induced collisions are the most frequent.[37,38]

Restitution coefficient including hydrodynamic effects

Local hydrodynamic interactions occuring during a collision lead to significant reduction of the particle relative velocity before and after impact on a length scale of the same order or shorter than the particle radius (see experiments for particles in glycerol solution[39,40] or drops in water[36]). Lubrication forces during the film drainage delay the physical contact and induce a strong dissipation of the kinetic energy of the particles involved in the collision. This can be viewed as an effective restitution coefficient related to the real inelasticity of the particle material supplemented by the local dissipation of the particle kinetic energy by the surrounding fluid. Legendre et al.[36] proposed an empirical law for the effective coefficient of restitution for a particle-wall collision $e_{pw} = e_0 \exp(-\frac{\beta}{St_\infty})$, where V_∞ is the velocity of the particle before its interaction with the wall and $St_\infty = \frac{m_p V_\infty}{6\pi\mu a^2}$ is the corresponding Stokes number (note that, unlike the standard definition used in the previous sections, St_∞ depends on the impact velocity of each individual collision). e_0 is the maximum restitution coefficient obtained in a dry collision and β an empirical parameter equal to 35.[36]

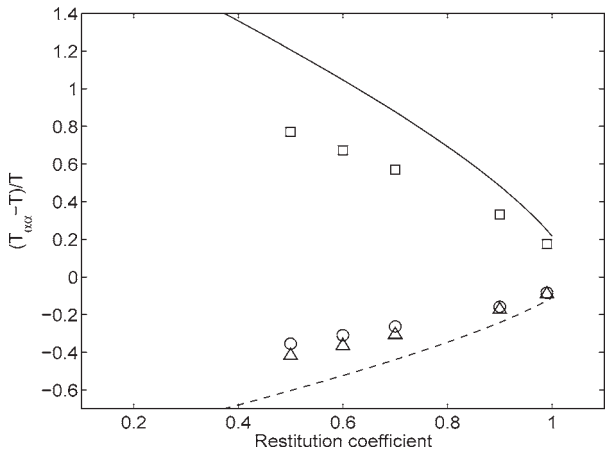

Figure 11. Normal stress difference $(T_{ij} - T\delta_{ij})/T$ vs. the restitution coefficient for $St = 5$ and $\phi = 15\%$.

The lines are obtained from the ignited theory. The solid line and squares stand for anisotropy in the flow direction. The circles, triangles, and dashed line stand for the anisotropy in the shear and spanwise directions.

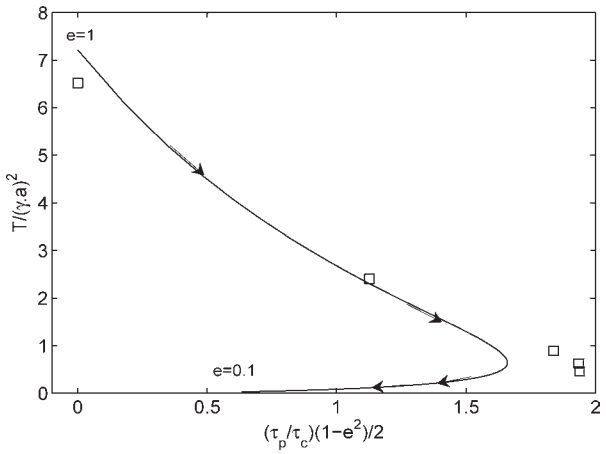

Figure 12. Granular temperature vs. the energy dissipation ratio (collisions/drag dissipations) for *St* = 5 and ϕ = 15%.

The solid line is obtained from the ignited theory. The arrows indicate the path corresponding to a reduction of the restitution coefficient from 1 to 0.1. The squares correspond to the simulations with e = 1, 0.9, 0.7, 0.6, 0.5 from top to bottom.

In the case of a collision of two identical particles, Yang and Hunt[40] found that the evolution of the restitution coefficient follows the same trend as for particle-wall collisions with a Stokes number based on a reduced particle mass m^* and radius a^* ($m^* = m_p$ and $a^* = a$ for particle-wall collisions whereas $m^* = m_p/2$ and $a^* = a/2$ for two-particle collisions). The effective particle–particle restitution coefficient e_{pp} depends on impact parameters and particle characteristics (24).

$$e_{pp} = e_0 \exp\left(-\frac{V_\beta}{V_{r,\infty}}\right) \tag{24}$$

where $V_\beta = \frac{\beta}{2}\frac{a}{\tau_p}$ and $V_{r,\infty}$ is the relative velocity of the two particles before collision.

The particle–fluid interaction can be modeled by two contributions: the standard drag force when particles are far apart from each others, and the direct hydrodynamic interaction (or lubrication effect) taken into account through the modification of the restitution coefficient (Eq. 24). Using this approach for pairwise hydrodynamic effect is only valid when the time scale of the drag force τ_p is much larger than the time scale of the lubrication forces τ_L.

In the ignited regime, the lubrication time scale can be estimated by $\tau_L = \frac{a}{2}\sqrt{\frac{\pi}{T}}$ as lubrication effects occur on a distance typically $O(2a)$[36] with a mean relative velocity $O(\sqrt{\frac{24}{\pi}T})$. The condition $\tau_p \gg \tau_L$ is then satisfied when $T/(\gamma^2 a^2) \gg \pi/(4St^2)$.

In the quenched state, the typical particle–particle relative velocity can be estimated by γa, therefore the condition $\tau_p \gg \tau_L$ leads to $St \gg 1$ in contradiction with the moderate particle inertia assumption. Consequently, the application of the proposed approach for direct hydrodynamic interaction modeling should be restricted to the ignited regime

Based on similar assumptions which were used in the higly agitated regime for the velocity distribution function ("Overview of Existing Theories" section), we obtain the distribution function of the relative velocity at impact **g.k**. Then, using Eq. 24 with $V_{r,\infty}$ =**g.k**, we can deduce the distribution of the restitution coefficient $f(e^*)$, with $e^* = e_{pp}/e_0$:

$$f(e^*) = -\frac{1}{T_\beta}\,\frac{1}{e^*\,ln^3(e^*)}\,\exp\left(-\frac{1}{4\,T_\beta\,ln^2(e^*)}\right) \tag{25}$$

where $T_\beta = \frac{T}{V_\beta^2} = \frac{4}{\beta^2}St^2\frac{T}{\gamma^2 a^2}$. The average restitution coefficient is obtained by integrating

$$<e_{pp}> = e_0\int_0^1 e^*\,f(e^*)\,de^* = 2\,e_0\int_0^{+\infty} u\,e^{-u^2}\,e^{-1/(2\,T_\beta^{1/2}u)}\,du \tag{26}$$

Assuming that $T_\beta \gg 1$, which is a reliable assumption for high Stokes numbers, an analytic expression for $<e_{pp}>$ is obtained by a Taylor expansion:

$$<e_{pp}> \simeq e_0\left(1 - \frac{1}{2}\sqrt{\frac{\pi}{T_\beta}}\right) \tag{27}$$

The validation of the theoretical expression of the restitution coefficient distribution Eq. 25 has been achieved by numerical simulations using a restitution coefficient depending on the relative velocities at impact (Eq. 24). We varied the Stokes number St = [5,10,50] and selected two volumetric concentrations of solid particles ϕ = [5,15]%. For all the simulations, the maximum restitution coefficient is $e_0 = 1$. Figure 13 compares the distribution functions of the restitution coefficient predicted by Eq. 25 with distributions obtained from simulations at $\phi = 5\%$ for St = 5, 10, and 50. On one hand, a very good agreement is achieved for both cases $St = 10$ and 50. On the other hand, large discrepancies are found for $St = 5$ which shows that the assumption of an ignited regime does not apply at this moderate Stokes number. When the Stokes number decreases, the particle agitation decreases, leading to a significant reduction of the mean restitution coefficient. The Figure 14 shows the effect of increasing the solid volume fraction on the distribution function of the restitution coefficient for $St = 10$. When the solid volume fraction increases the particle agitation decreases, leading to a decrease of the mean restitution coefficient, as predicted by Eq. 27.

Furthermore, we accounted for the dependance of the restitution coefficient on the relative velocity in the transport equations of agitation and kinetic stresses (in both the quenched and agitated regimes). In the ignited regime, this leads to the modification of the collisional terms χ_{ij} and θ_{ij}, where the coefficient of restitution has to be multiplied by correction prefactors R_{np} defined by:

$$R_{np} = \left(\frac{1}{I_n}\int_0^{+\infty} e^{-p/(2\,T_\beta^{1/2}u)}\,u^n\,e^{-u^2}\,du\right)^{\frac{1}{p}} \tag{28}$$

with I_n are constants defined by $I_n = \int_0^{+\infty} u^n e^{-u^2} du$

The overall energy dissipation induced by the particle collisions is:

$$\frac{\chi_{ii}}{2} = -\frac{T}{2}\,\frac{\phi\,\rho_p}{\tau_c}\left(1 - (R_{32}\,e_0)^2\right) \tag{29}$$

Assuming that R_{np} has an exponential form, a first-order Taylor expansion of Eq. 28 yields $R_{np} \simeq e^{-I_{n-1}/(2I_n T_\beta^{1/2})} = R_n$. Therefore, the energy dissipation can be approximated by Eq. 30. For more details of the modification of the ignited theory the reader is referred to Appendix.

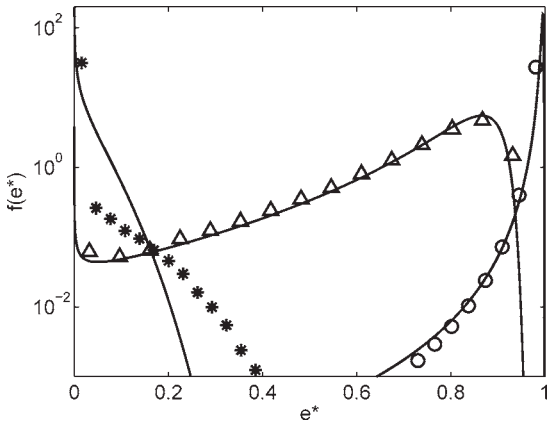

Figure 13. Probability density function of the restitution coefficient depending on the impact velocities for ϕ = 5%.

The solids lines are obtained from Eq. 25. ○, Δ, and * correspond to numerical simulations for St = 50, 10, and 5, respectively.

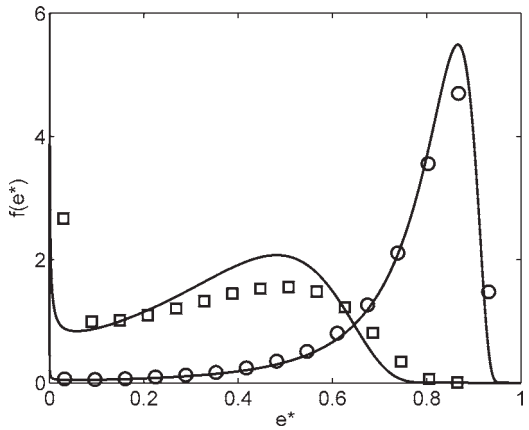

Figure 14. Probability density functions of the restitution coefficient depending on the impact velocities for *St* = 10.

The solids lines are obtained from Eq. 25. ○ and □ correspond to numerical simulations for ϕ = 5% and 15%, respectively.

$$\frac{\chi_{ii}}{2} \simeq -\frac{T}{2}\,\frac{\phi\,\rho_{\mathrm{p}}}{\tau_{\mathrm{c}}}\,\left(1-(R_3\,e_0)^2\right) \tag{30}$$

The equations governing the quenched regime can also be extended following the same approach. In this case, the particle agitation is given by the following equation:

$$\frac{T}{\gamma^2 a^2} = \frac{1}{6}\,St\,C_{ii} - \frac{1}{6}\,St^2\,C_{12} + \frac{1}{12}\,St^3 C_{22} \tag{31}$$

where the terms C_{ij} denote the collisional terms equal to:

$$C_{ij} = -\frac{6}{\pi}\,\phi g_0\,I_{ij}\,\left(1+2\,Q_{ij}(St)\,e_0 + Q_{ij}(St/2)\,e_0^2\right) \tag{32}$$

where I_{ij} is constant defined by $I_{ij} = \int_{k_x k_y\,<0} (k_x\,k_y)^3\,k_i\,k_j\,\mathbf{dk}$ and Q_{ij} is obtained by:

$$Q_{ij} = \frac{1}{I_{ij}}\int_{k_x k_y<0} \exp\left(\frac{\beta}{4\,St\,k_x k_y}\right)\,(k_x k_y)^3\,k_i k_j\,\mathbf{dk} \tag{33}$$

Assuming $Q_{ij} \simeq \exp(-\frac{\beta}{4}\frac{a_{ij}}{St})$, a first-order Taylor expansion yields an analytic expression for the symmetric tensor a_{ij} in Q_{ij} ($a_{11} = a_{22} = \frac{27\pi}{32}, a_{33} = \frac{9\pi}{8}, a_{12} = \frac{8}{\pi}$ and $a_{13} = a_{23} = 0$). Finally, the collisional terms are obtained by:

$$C_{ij} \simeq -\frac{6}{\pi}\,\phi g_0\,I_{ij}\,\left(1+\,Q_{ij}(St)\,e_0\right)^2 \tag{34}$$

Figure 15 shows the evolution of the particle agitation with concentration for St = 5, 10, and 50. The numerical results are compared with the corresponding modified theory. A very good agreement is obtained for St = 50 for any concentration and for St = 5 and 10 at low concentration (i.e., ϕ = 5%). Figure 15 also shows the theoretical predictions for perfectly elastic collisions e = 1. Compared with the reference case e = 1, the level of particle agitation is significantly reduced when the restitution coefficient is dynamically evaluated: for instance when St = 50, the level of agitation is reduced by a factor of 4 and 25 for ϕ = 5% and ϕ = 15%, respectively.

Figure 16 shows the dependence of the effective restitution coefficient $R_3\,e_0$ (appearing in χ_{ii}, Eq. 30) on the Stokes number for several particle concentrations. At large Stokes number, the effecive restitution coefficient tends asymptotically toward e_0. For St = 50, the effective restitution coefficient is equal to 0.995 e_0 and 0.98 e_0, respectively, for ϕ = 5% and ϕ = 15%.

A comparison of the energy dissipation ratio (collision/drag dissipations) is presented in Figure 17 for the standard (constant restitution coefficient) and extended ignited theory (i.e., variable restitution coefficient). For ϕ = 5%, we considered particularly two cases corresponding to maximum restitution coefficients e_0 = 1 and e_0 = 0.9. In the case e_0 = 1, St = 50, and ϕ = 5%, both dissipation mechanisms (inelastic collisions and drag) are of the

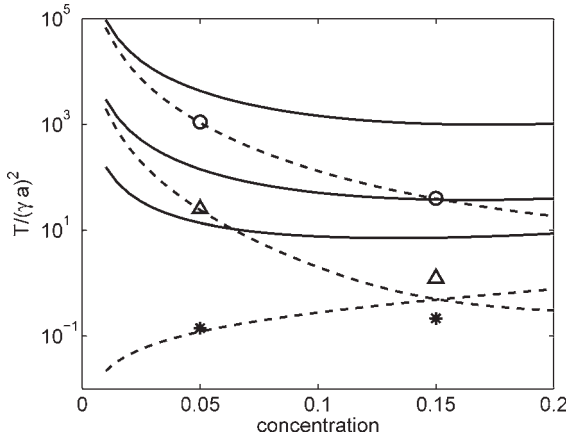

Figure 15. Particle agitation vs. concentration for different Stokes numbers.

Symbols (○, Δ, and * correspond, respectively, to St = 50, 10, and 5) stand for the numerical results with β = 35. Solid lines (from top to bottom: St = 50, 10, and 5) correspond to the theoritical prediction of the standard ignited theory. Dashed lines (from top to bottom: St = 50, 10, and 5) correspond to the theoritical prediction of the modified ignited theory for St = 50 and St = 10 and of the modified quenched theory for St = 5.

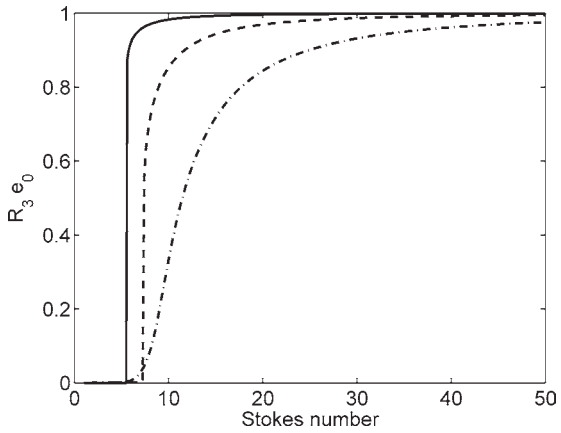

Figure 16. Effective coefficient of restitution $R_3\ e_0$ vs. Stokes number for different particle concentrations for $e_0 = 1$.

The solid, dashed, and dash-dotted lines correspond to $\phi = 5$, 10, and 15%, respectively.

same magnitude. This explains why a very weak variation of the effective restitution coefficient (i.e., 0.5% for that case) has a dramatic effect on the particle agitation (reduced by a factor of 4 compared with the reference case). However when $e_0 = 0.9$, the trend of the dissipation ratio increase is similar when the restitution coefficient is constant or varies with the impact parameters (at $St = 50$ there is only a 10% difference). This means that the modeling of direct hydrodynamic interactions has a weak influence on the particle agitation for inelastic particles.

Unexpectedly, when $e_0 = 1$ the energy dissipation ratio is constant when $St > 10$. Assuming that $T_\beta \gg 1$, the ratio of energy dissipation can be expressed as:

$$\frac{1}{2}\frac{\tau_p}{\tau_c}\left(1-(R_{32}\,e_0)^2\right) \simeq \frac{1}{2}\frac{\tau_p}{\tau_c}\,(1-e_0^2)+\frac{3}{2}\,\phi\,g_0\,e_0^2\,\beta \quad (35)$$

Equation 35 shows that in the particular case of $e_0 = 1$ the dissipation ratio is asymptotically independent of St. However, the magnitude of the dissipation ration is proportional to ϕg_0 which accounts for the effect of dense suspensions.

Conclusion

The dynamics of a suspension composed by particles with finite inertia suspended in a sheared viscous fluid flow has been investigated. We assumed that Brownian motion and fluid inertia effects were negligible. Typical suspensions satisfying such conditions consist in solid millimetric particles [$a = O(0.1 - 1)$mm] embedded in a gas flow. The prediction of the bulk properties needs a fundamental understanding of the interaction between the solid and the fluid phases. The simple configuration of a pure linear shear flow has been chosen as a prototype configuration involving a velocity gradient. Although the gravity effect is present in real situations, we neglected the mean settling of the particles to emphasize the shear induced interactions. Hindering effect due to local hydrodynamic interactions between neighboring particles has been also neglected but may be easily modeled by an effective drag coefficient[17]). We proposed an alternative modeling based on an effective restitution coefficient accounting for the presence of the interstitial fluid. The suspension inertia is characterized by a macroscopic Stokes number, which is the ratio of the characteristic times related to the particulate viscous relaxation and to the shear rate of the flow. Discrete particle simulations were carried out for testing theory prediction (a statistical approach based on the kinetic theory of granular flow).

First, we investigated the macroscopic behavior of suspensions with perfectly elastic rebounds. The dynamic equilibrium results from a balance between the energy input by the shear and the drag force dissipation. The simulations performed for $St = 1$ to 10 showed that in this range of moderate particle inertia the suspension dynamics was extremely rich evolving from a quenched to a highly agitated regime. For a fixed concentration, the particle agitation increases dramatically with the Stokes number. For inertial particles or moderate concentration, the velocity distributions were found to follow a deviated Maxwellian shape, leading to an excellent agreement between the simulations and the theory which is an extension of the classical kinetic theory[8] including drag dissipation.[17–19] In that case, momentum transfer is driven by successive collisions of the particles. However, for low particle inertia and dilute suspension, the velocity distributions of the velocity fluctuations are highly peaked around zero, indicating that most collisions are shear-induced. The particle recovers the fluid streamline on a short time after the collision. In this limit, the particle agitation tensor was found to follow the so-called quenched theory developed by Tsao and Koch[19] based on an assumption of a Dirac function for the velocity distribution. A general solution could be envisaged as a gradual combination of the two theories (Dirac function and deviated Maxwellian function) for intermediate regimes.

Both kinetic and collisional contributions to the stress were computed in the normal and shear directions. The appropriate theory for predicting the particle agitation leads in most of the cases to a very accurate estimate. All the stress contributions were found to increase with concentration in the quenched regime. The high anisotropy found in the quenched regime (significant normal stress difference $(T_{11} - T)/T \approx 1$) decreased strongly when the collision effects become dominant over the drag contribution.

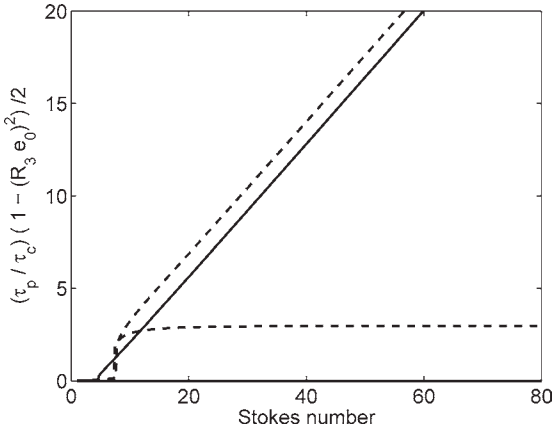

Figure 17. Ratio of the two mechanisms of energy dissipation (collision/drag) vs. Stokes number for $\phi = 5\%$.

The solid line corresponds to the standard ignited theory with $e = 0.9$. Dashed lines (from top to bottom: $e_0 = 0.9$ and $e_0 = 1$) correspond to the modified ignited theory.

Concentrated suspensions were found to always behave as a dry granular material where most of the momentum transfer occurs through collisions. The effective viscosity deduced from the shear stress contributions was compared with a viscosity model commonly used for gas–solid suspension flows. The agreement was very good in highly agitated suspensions where an assumption of weak anisotropy is valid. But this model may be flawed for the quenched regime of sheared suspensions (low Stokes and concentration).

The sensitivity of the results to inelasticity was evaluated by simulations with constant particle inertia and varying restitution coefficient. A significant modification of the macroscopic behavior of highly inertial particles appeared when the restitution coefficient decreased from 1 to 0.5 (for $St = 5$, the particle agitation was decreased roughly by one order of magnitude), whereas no significant variation was observed for weakly inertial particles. Additionally, we propose a simple modeling of local hydrodynamic interactions occuring during each binary collision. We modeled the damping effect of the fluid drainage by an equivalent restitution coefficient which depends on the instantaneous particle impact velocities. The instantaneous restitution coefficient is related to the binary Stokes number based on impact parameters (Legendre et al.[36], Yang and Hunt[40]). The predictions based on the kinetic theory for the ignited and quenched states were extended to take into account this effect. We have found a very good agreement with numerical simulations at low concentration (i.e., $\phi = 5\%$). At moderate concentration (i.e., $\phi = 15\%$), the theory is very efficient for high Stokes number. The distribution of the restitution coefficient was compared with the assumption used in the theory as a validation step. This helps to limit the range of accuracy of our statistical approach. At high Stokes numbers, the effective restitution coefficient is slightly different from the reference case. Including the effect of binary hydrodynamic interactions leads to more pronounced effects at moderately concentrated to dense suspensions or moderate Stokes numbers.

Acknowledgments

Simulations were performed on our regional supercomputing center Calmip–CICT. They are gratefully acknowledged. The authors would also like to acknowledge Total CReG who supported a part of this work. J.F.P thanks M. Linkés for fruitful discussions.

Literature Cited

1. Jiradilok V, Gidaspow D, Damronglerd S, Koves J, Mostofi R. Kinetic theory based cfd simulation of turbulent fluidization of fcc particles in a riser. *Chem Eng Sci.* 2006;61:5544–5559.
2. Li J, Kuipers J. Effect of competition between particle-particle and gas-particle interactions on flow patterns in dense gas-fluidized beds. *Chem Eng Sci.* 2007;62:3429–3442.
3. Zhu H, Zhou Z, Yang R, Yu A. Discrete particle simulation of particulate systems: a review of major applications and findings. *Chem Eng Sci.* 2008;63:5728–5770.
4. Deen N, Annaland MVS, der Hoef MV, Kuipers J. Review of discrete particle modeling of fluidized beds. *Chem Eng Sci.* 2007;62:28–40.
5. Hoomans B, Kuipers J, Briels W, Swaaij WV. Discrete particle simulation of bubble and slug formation in a two-dimensional gas-fluidized bed: a hard-sphere approach. *Chem Eng Sci.* 1996;51:99–118.
6. Koch D, Hill R. Inertial effects in suspensions and porous-media flows. *Ann Rev Fluid Mech.* 2001;33:619–647.
7. Ding J, Gidaspow D. A bubbling fluidization model using kinetic theory of granular flow. *AICHE J.* 1990;36:523–538.
8. Chapman S, Cowling T. *The Mathematical Theory of Non-Uniform Gases*. Cambridge, U.K.: Cambridge University Press, 1970.
9. Ogawa S, Umemura A, Oshima N. On the equations of fully fluidized granular material. *J Appl Math Phys.* 1980;31:483–493.
10. Savage S, Jeffrey J. The stress tensor in a granular flow at high shear rates. *J Fluid Mech.* 1981:110:255–272.
11. Abbas M, Climent E, Simonin O, Maxey M. Dynamics of bidisperse suspensions under stokes flows: Linear shear flow and sedimentation. *Phys Fluids*. 2006;18:1–20.
12. Breedveld V, den Ende DV, Tripathi A, Acrivos A. The measurement of the shear-induced particle and fluid tracer diffusivities by a novel method. *J Fluid Mech.* 1998;375:297–318.
13. Sierou A, Brady J. Shear-induced self-diffusion in non-colloidal suspensions. *J Fluid Mech.* 2004;506:285–315.
14. Acrivos A, Batchelor G, Hinch E, Koch D, Mauri R. Longitudinal shear-induced diffusion of spheres in a dilute suspension. *J Fluid Mech.* 1992;240:651–657.
15. Jenkins J, Richman M. Grad's 13-moment system for a dense gas of inelastic spheres. *Ar Rat Mech Anal.* 1985;87:355–377.
16. Grad H. On the kinetic theory of rarified gas. *Commun Pure Appl Math.* 1949;2:331–407.
17. Sangani A, Mo G, Tsao H, Koch D. Simple shear flows of dense gas-solid suspensions at finite stokes numbers. *J Fluid Mech.* 1996; 313:109–341.
18. Boelle A, Balzer G, Simonin O. Second-order prediction of the particle-phase stress tensor of inelastic spheres in simple shear dense suspensions. *Proceedings of Sixth International Symposium on Gas-Solid Flows.* 1995;228:9.
19. Tsao H, Koch D. Simple shear flows of dilute gas-solid suspensions. *J Fluid Mech.* 1995;296:211–245.
20. Kulkarni P, Morris J. Suspension properties at finite reynolds number from simulated shear flow. *Phys Fluids.* 2008;20:1–13.
21. Verberg R, Koch D. Rheology of particle suspensions with low to moderate fluid inertia at finite particle inertia. *Phys Fluids.* 2006; 18:1–16.
22. Xu H, Verberg R, Koch D, Louge M. Dense, bounded shear flows of agitated solid spheres in a gas at intermediate stokes and finite reynolds numbers. *J Fluid Mech.* 2009;618:181–208.
23. Ergun S. Flow through packed columns. *Chem Eng Prog.* 1952;48:89.
24. Wen C, Yu Y. Mechanics of fluidization. *Chem Eng Prog.* 1966;62:100.
25. Beetstra R, van der Hoef M, Kuipers J. Drag force of intermediate reynolds number flow past mono- and bidisperse arrays of spheres. Fluid Mechanics and Transport Phenomena. *AICHE.* 2007;53:489–501.
26. Lun C, Savage S. The effects of an impact velocity dependent coefficient of restitution on stresses developed by sheared granular materials. *Acta Mechanica.* 1986;63:15–44.
27. Wylie J, Koch D, Ladd A. Rheology of suspensions with high particle inertia and moderate fluid inertia. *J Fluid Mech.* 2003;480:95–118.
28. Allen MP, Tildesley DJ. *Computer Simulations of Liquids*. Oxford, U.K.: Oxford University Press, 1987.
29. Campbell C. Rapid granular flows. *Ann Rev Fluid Mech.* 1990; 22:57.
30. Sundaram S, Collins L. Numerical considerations in simulating a turbulent suspension finite-volume particles. *J Comp Phys.* 1996; 124:337–350.
31. Abbas M, Climent E, Simonin O. Shear-induced self-diffusion of inertial particles in a viscous fluid. *Phys Rev E.* 2009;79:1–8.
32. Balzer G, Boelle A, Simonin O. Eulerian gas-solid flow modelling of dense fluidized bed. *Proceedings of Sixth International Symposium on Gas-Solid Flows*, ASME FEDSM, 1995;409–418.
33. Gobin A, Neau H, Simonin O, Llinas J, Reiling V, Sélo J. Fluid dynamic numerical simulation of a gas phase polymerisation reactor. *Int J Num Meth Fluids.* 2003;43:1199–1220.
34. Campbell C. Self-diffusion in granular shear flows. *J Fluid Mech.* 1997;348:85–101.
35. Lutsko J, Brey J, Dufty W. Diffusion in a granular fluid. II. Simulation. *Phys Rev E.* 2002;65:1–10.
36. Legendre D, Zenit R, Daniel C, Guiraud P. A note on the modelling of the bouncing of spherical drops or solid spheres on a wall in viscous fluid. *Chem Eng Sci.* 2006;61:3543–3549.
37. Hopkins M, Louge M. Inelastic microstructure in rapid granular flows of smooth disks. *Phys Fluids A.* 1991;3:47–57.

38. Alam M, Luding S. Energy nonequipartition, rheology, and microstructure in sheared bidisperse granular mixtures. *Phys Fluids*. 2005;17:1–18.
39. Joseph G, Zenit R, Hunt M, Rosenwikel A. Particle-wall collision in a viscous fluid. *J Fluid Mech*. 2001;433:329–346.
40. Yang F, Hunt M. Dynamics of particle-particle collisions in a viscous liquid. *Phys Fluids*. 2006;18:1–11.

Appendix

Modified ignited theory

In the framework proposed by Jenkins and Richman,[15] the collisional terms can be written as:

$$C(\Psi) = \chi(\Psi) - \frac{\partial}{\partial x_j}\Theta_j(\Psi) \tag{A1}$$

$\chi(\Psi)$ and $\theta_k(\Psi)$ are defined by:

$$\chi(\Psi) = 2\,a^2 g_0 \int\int\int_{\mathbf{g},\mathbf{k}>0} \Delta(\Psi)\, f(\mathbf{c_1},\mathbf{x}) f(\mathbf{c_2},\mathbf{x}) \times \left(1 + a\, k_i \frac{\partial}{\partial x_i} ln\left(\frac{f(\mathbf{c_2},\mathbf{x})}{f(\mathbf{c_1},\mathbf{x})}\right)\right)(\mathbf{g}\cdot\mathbf{k}) d\mathbf{k}\, d\mathbf{c_1} d\mathbf{c_2} \tag{A2}$$

$$\Theta_j(\Psi) = -4\,a^3 g_0 \int\int\int_{\mathbf{g}.\mathbf{k}>0} \delta(\Psi_1)\, f(\mathbf{c_1},\mathbf{x}) f(\mathbf{c_2},\mathbf{x}) \times \left(1 + a\, k_i \frac{\partial}{\partial x_i} ln\left(\frac{f(\mathbf{c_2},\mathbf{x})}{f(\mathbf{c_1},\mathbf{x})}\right)\right)(\mathbf{g}\cdot\mathbf{k}) k_j\, d\mathbf{k}\, d\mathbf{c_1} d\mathbf{c_2} \tag{A3}$$

with $\Delta(\Psi)$ the variation of Ψ during the collision of two particles and $\delta(\Psi_1)$ the variation of Ψ for the particle of velocity $\mathbf{c_1}$.

Then, χ_{ij} and Θ_{ij} are defined by:

$$\chi_{ij} = \chi(m_p c_i c_j) \tag{A4}$$

$$\Theta_{ij} = \Theta_j(m_p c_i) \tag{A5}$$

Based on the simple laws for a binary collision, we obtain:

$$\delta(m_p\, \mathbf{c_1}) = -\frac{1}{2}\,(1+e_{pp})\,(\mathbf{g}\cdot\mathbf{k})\,\mathbf{k} \tag{A6}$$

$$\Delta(m_p\, c_i\, c_i) = \frac{1}{2}\,(1+e_{pp})\,\left((1+e_{pp})(\mathbf{g}\cdot\mathbf{k})\,k_i k_j - (k_i g_j + k_j g_i)\right) \tag{A7}$$

with $\mathbf{g} = \mathbf{c_1} - \mathbf{c_2}$ and $\mathbf{k} = \mathbf{x_2} - \mathbf{x_1}$. We can then derive the expressions for χ_{ij} and Θ_{ij}. The only modification of the study of Jenkins and Richman[15] is that e_{pp} is now a function of $(\mathbf{g}\cdot\mathbf{k})$:

$$e_{pp} = e_0 \exp\left(-\frac{V_\beta}{\mathbf{g}\cdot\mathbf{k}}\right) \tag{A8}$$

where $V_\beta = \frac{\beta}{2}\frac{a}{\tau_p}$. Integrating the collisional terms χ_{ii}, χ_{22}, χ_{12}, Θ_{22}, and Θ_{12} gives:

$$\chi_{ii} = -T\,\frac{\phi\,\rho_p}{\tau_c}\left(1 - (R_{32}\,e_0)^2\right) \tag{A9}$$

$$\begin{aligned}\chi_{22} = {} & \frac{1}{3}\,\frac{\phi\,\rho_p}{\tau_c} T\left(1 + 2\,R_{31}\,e_0 + (R_{32}\,e_0)^2\right) - \frac{2}{3}\,\frac{\phi\,\rho_p}{\tau_c} T(1 + R_{31}\,e_0) \\ & + \frac{4}{15}\,\frac{\phi\,\rho_p}{\tau_c}\,\hat{T}_{22}\left(1 + 2\,R_{51}\,e_0 + (R_{52}\,e_0)^2\right) \\ & - \frac{1}{15}\,\frac{\phi\,\rho_p}{\tau_c}\,\hat{T}_{22}\left(1 + 2\,R_{31}\,e_0 + (R_{32}\,e_0)^2\right) \\ & - \frac{8}{15}\,\frac{\phi\,\rho_p}{\tau_c}\,\hat{T}_{22}\,(1 + R_{51}\,e_0) - \frac{4}{15}\,\frac{\phi\,\rho_p}{\tau_c}\,\hat{T}_{22}\,(1 + R_{31}\,e_0)\end{aligned} \tag{A10}$$

$$\begin{aligned}\chi_{12} = {} & \frac{12}{5}\,\phi\,\rho_p\,\phi\,g_0\,T\,\hat{D}_{p,12}\,(2\,(1 + R_{41}\,e_0) + (1 + R_{21}\,e_0)) \\ & - \frac{12}{5}\,\phi\,\rho_p\,\phi\,g_0\,T\,\hat{D}_{p,12}\left(1 + 2\,R_{41}\,e_0 + (R_{42}\,e_0)^2\right) \\ & + \frac{4}{15}\,\frac{\phi\,\rho_p}{\tau_c}\,\hat{T}_{12}\left(1 + 2\,R_{51}\,e_0 + (R_{52}\,e_0)^2\right) \\ & - \frac{1}{15}\,\frac{\phi\,\rho_p}{\tau_c}\,\hat{T}_{12}\left(1 + 2\,R_{31}\,e_0 + (R_{32}\,e_0)^2\right) \\ & - \frac{8}{15}\,\frac{\phi\,\rho_p}{\tau_c}\,\hat{T}_{12}\,(1 + R_{51}\,e_0) - \frac{4}{15}\,\frac{\phi\,\rho_p}{\tau_c}\,\hat{T}_{12}\,(1 + R_{31}\,e_0)\end{aligned} \tag{A11}$$

$$\begin{aligned}\Theta_{22} = {} & 2\,\phi\,\rho_p\,\phi\,g_0\,T\,(1 + R_{21}\,e_0) \\ & + \frac{4}{10}\,\phi\,\rho_p\,\phi\,g_0\,\hat{T}_{22}\,(3\,(1 + R_{41}\,e_0) - (1 + R_{21}\,e_0))\end{aligned} \tag{A12}$$

$$\begin{aligned}\Theta_{12} = {} & \frac{4}{10}\,\phi\,\rho_p\,\phi\,g_0\,\hat{T}_{12}\,(3\,(1 + R_{41}\,e_0) - (1 + R_{21}\,e_0)) \\ & - \frac{16}{5}\,\phi\,\rho_p\,\phi\,g_0\,a\,\sqrt{\frac{T}{\pi}}\,\hat{D}_{p,12}\,(1 + R_{31}\,e_0)\end{aligned} \tag{A13}$$

where $\hat{D}_{p,ij}$ the anisotropic part of the tensor $D_{p,ij} = \frac{1}{2}\left(\frac{\partial U_{p,i}}{\partial x_j} + \frac{\partial U_{p,j}}{\partial x_i}\right)$ and $\hat{T}_{ij} = Ta_{ij}$. R_{np} are functions of T_β defined by:

$$R_{np} = \left(\frac{1}{I_n}\int_0^{+\infty} e^{-p/(2\,T_\beta^{1/2}u)}\,u^n\,e^{-u^2}\,du\right)^{\frac{1}{p}} \tag{A14}$$

where $T_\beta = \frac{T}{V_\beta^2}$.

Manuscript received July 28, 2009, and revision received Jan. 6, 2010.